Variance of Cone-beam Pair-wise Consistency Conditions in Helical CT

Mélanie Mouchet, Simon Rit, Jérôme Lesaint, Jean Michel Létang

Variance of cone-beam pair-wise consistency conditions in helical CT

Mélanie Mouchet, Simon Rit, Jérome Lesaint and Jean Michel Létang

***Abstract*—Data consistency conditions (DCC) are mathematical equations characterizing the redundancy in X-ray projections. They have been successfully used to calibrate the scanner geometry or correct projections (e.g. for beam hardening or scatter). Evaluating the DCC implies the computation of moments of the projections. Since the projections are subject to random noise, DCC will be as well. Accounting for this uncertainty would likely improve DCC-based algorithms which estimate some model parameters by maximizing the consistency between projections. In this work, we calculate the variance of DCC assuming known and uncorrelated noise in the projection pixels, following the approach used to compute noise in computed tomography (CT) images reconstructed with a filtered-backprojection algorithm. The DCC are computed between pairs of cone-beam projections acquired on a helical trajectory. The variance formula was validated with batch simulations. Large noise differences were observed in this set of DCC, up to two orders of magnitude, which demonstrates that it is crucial to account for this noise in DCC-based algorithms.**

***Index Terms*—statistical noise, data consistency conditions, helical CT**

I. Introduction

Data consistency conditions (DCC) are mathematical equations that must be verified by the measured data. DCC are mainly used to geometrically calibrate the scanner or reduce image artifacts in computed tomography (CT). These DCC-based algorithms rely on the minimization of a cost function defined from the DCC. To our knowledge, while there have been many papers on DCC and their applications, none has considered the statistical nature of the input data. However, as previously shown for iterative reconstruction algorithms minimizing weighted least squares from low-dose X-ray projections [1], accounting for the variance of the DCC in the cost function could increase the robustness of DCC-based algorithms.

The main goal of this work is to derive the noise of cone-beam pair-wise DCC in helical CT assuming known and uncorrelated noise in projection pixels. The derivation follows the approach used to calculate the noise in CT images reconstructed with filtered backprojection algorithms, e.g. in [2].

Mélanie Mouchet is with Siemens Healthcare, Paris, France and Université de Lyon, CREATIS; CNRS UMR5220; Inserm U1044; INSA-Lyon; Université Lyon 1; Centre Léon Bérard, France.

Jerome Lesaint, Jean Michel Létang and Simon Rit are with Université de Lyon, CREATIS; CNRS UMR5220; Inserm U1044; INSA-Lyon; Université Lyon 1; Centre Léon Bérard, France.

II. Methods

A. Cone-beam pair-wise DCC in helical CT

Let $\boldsymbol{s}_\lambda$ and $\boldsymbol{s}_{\lambda'}$ be two source positions on a helical trajectory and g_λ and $g_{\lambda'}$ the corresponding two-dimensional (2D) cone-beam projections as illustrated in Figure 1. The detector is cylindrical of radius D. A detector pixel is defined by its cylindrical coordinates (γ, v) in the detector frame with $\gamma \in [-\gamma_{\max}, \gamma_{\max}]$ and $v \in [-v_{\max}, v_{\max}]$. Let $\Pi_{\boldsymbol{\tau}}$ be a plane containing the two source positions $\boldsymbol{s}_\lambda$ and $\boldsymbol{s}_{\lambda'}$, where $\boldsymbol{\tau} = (\lambda, \lambda', \beta)$ characterizes this plane and $\beta \in (-\pi/2, \pi/2)$ is the angle with a chosen reference plane noted $\Pi_{\lambda,\lambda'}$ [3]. We only consider source pairs $(\boldsymbol{s}_\lambda, \boldsymbol{s}_{\lambda'})$ which define a so-called *baseline* which is not parallel to the axis of the source helix and we note $\boldsymbol{b}_{\lambda,\lambda'} = (b_1, b_2, b_3) = \operatorname{sign}(\lambda' - \lambda)\dfrac{\boldsymbol{s}_{\lambda'} - \boldsymbol{s}_\lambda}{\|\boldsymbol{s}_{\lambda'} - \boldsymbol{s}_\lambda\|}$ the baseline direction. The plane $\Pi_{\boldsymbol{\tau}}$ intersects the projection g_λ along a curve with a parametric equation $v_{\boldsymbol{\tau}}(\gamma)$. We define the moment of the projection g_λ

$$M_{\boldsymbol{\tau}} = \int_{-\gamma_{\max}}^{\gamma_{\max}} \frac{\operatorname{sign}(\gamma_s)\pi D h(\gamma_s - \gamma)}{\sqrt{b_1^2 + b_2^2}\sqrt{D^2 + v_{\boldsymbol{\tau}}(\gamma)^2}} \frac{g_\lambda(\gamma, v_{\boldsymbol{\tau}}(\gamma))}{\operatorname{sinc}(\gamma_s - \gamma)} \mathrm{d}\gamma \tag{1}$$

where γ_s is the detector angle at which the baseline and the detector cylinder at g_λ intersect, and h is the Hilbert kernel defined by $h(\gamma) = 1/(\pi\gamma)$. Equation 1 was obtained by a suitable change of variable in the zero-th order moment used for fan-beam DCC with sources on a line [4] after observing that the intersection of $\Pi_{\boldsymbol{\tau}}$ with g_λ and $g_{\lambda'}$ results in two fan-beam projections with the corresponding sources on the baseline. If these two fan-beam projections are untruncated,

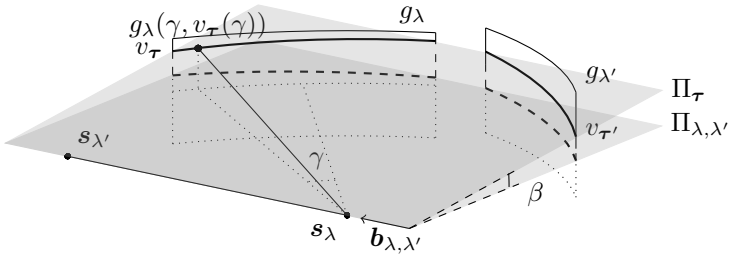

Fig. 1: Illustration of the cone-beam pair-wise geometry.

the DCC state that $M_{\boldsymbol{\tau}} = M_{\boldsymbol{\tau}'}$ with $\boldsymbol{\tau}' = (\lambda', \lambda, \beta)$ ($M_{\boldsymbol{\tau}'}$ is therefore a moment of the projection $g_{\lambda'}$). We sample B planes with the same baseline (B depends on the overlap between the two FOVs), define the mean moment over the B planes

$$\overline{M_{\lambda,\lambda'}} = \frac{1}{B}\sum_{b=1}^{B} M_{\boldsymbol{\tau}_b} \tag{2}$$

and build our cone-beam pair-wise consistency metric $|\overline{M_{\lambda,\lambda'}} - \overline{M_{\lambda',\lambda}}|$.

B. Discretization

The detector is made of $N_{\text{cols}} \times N_{\text{rows}}$ such that γ and v are discretized as $\gamma_i = -\gamma_{\max} + (i-1)\Delta_\gamma, i \in \{1, ..., N_{\text{cols}}\}$ and $v_j = -v_{\max} + (j-1)\Delta_v, j \in \{1, ..., N_{\text{rows}}\}$. The discretization of Equation 1 yields

$$M_{\boldsymbol{\tau}} \simeq \sum_{i=1}^{N_{\text{cols}}} a_{\boldsymbol{\tau}}(\gamma_i) g_\lambda(\gamma_i, v_{\boldsymbol{\tau}}(\gamma_i)), \tag{3}$$

$$a_{\boldsymbol{\tau}}(\gamma_i) = \frac{\text{sign}\,(\gamma_s)\pi D h_\nu(\gamma_s - \gamma_i)}{\sqrt{b_1^2 + b_2^2}\sqrt{D^2 + v_{\boldsymbol{\tau}}(\gamma_i)^2}} \frac{1}{\text{sinc}(\gamma_s - \gamma_i)} \Delta_\gamma \tag{4}$$

where

$$h_\nu(\gamma) = \frac{1 - \cos(\nu \frac{\pi\gamma}{\Delta_\gamma})}{2\pi\gamma} + \frac{\gamma(1 + \cos(\nu \frac{\pi\gamma}{\Delta_\gamma}))}{2\pi(\gamma^2 - \frac{\Delta_\gamma^2}{\nu^2})} \tag{5}$$

are the coefficients after discretization of a band-limited version of $h(\gamma_s - \gamma)$ using a Hann window and $\nu \in (0, 1]$ characterizes a fraction of Nyquist's frequency for the discretization in the ν direction and controls the bandwidth of the kernel. $v_{\boldsymbol{\tau}}(\gamma_i) \in [v_j, v_{j+1})$ is the detector axial coordinate of the intersection between $\Pi_{\boldsymbol{\tau}}$ and the projection column $\gamma = \gamma_i$. The value of $g_\lambda(\gamma_i, v_{\boldsymbol{\tau}}(\gamma_i))$ is obtained by linear interpolation

$$g_\lambda(\gamma_i, v_{\boldsymbol{\tau}}(\gamma_i)) \simeq (1 - w_{i,j}) g_\lambda(\gamma_i, v_j) + w_{i,j} g_\lambda(\gamma_i, v_{j+1}) \tag{6}$$

where

$$w_{i,j} = \frac{v_{\boldsymbol{\tau}}(\gamma_i) - v_j}{\Delta_v} \tag{7}$$

is the linear interpolation weight.

C. Variance formula of the consistency metric

The variance of difference of the mean moments is given by

$$\text{Var}\left(\overline{M_{\lambda,\lambda'}} - \overline{M_{\lambda',\lambda}}\right) = \text{Var}\left(\overline{M_{\lambda,\lambda'}}\right) + \text{Var}\left(\overline{M_{\lambda',\lambda}}\right) \tag{8}$$

as the two mean moments $\overline{M_{\lambda,\lambda'}}$ and $\overline{M_{\lambda',\lambda}}$ are uncorrelated because they apply to two different projections. To express $\text{Var}\left(\overline{M_{\lambda,\lambda'}}\right)$ in terms of the noise of the projection pixels $\text{Var}\left(g_\lambda(\gamma, v)\right) \simeq 1/(I_0 \exp(-g_\lambda(\gamma, v)))$, I_0 being the incident number of photons, we assume that the projection pixels are uncorrelated [2]. Yet, two moments $M_{\boldsymbol{\tau}_k}$ and $M_{\boldsymbol{\tau}_l}$ may use the same pixels of the projection g_λ and be correlated, which is accounted for by computing the co-variance $\text{Cov}\left(M_{\boldsymbol{\tau}_k}, M_{\boldsymbol{\tau}_l}\right)$. The variance of the mean moment is

$$\begin{aligned}\text{Var}\left(\overline{M_{\lambda,\lambda'}}\right) = &\frac{1}{B^2} \sum_{b=1}^{B} \text{Var}\left(M_{\boldsymbol{\tau}_b}\right) \\ &+ \frac{2}{B^2} \sum_{1 \le k < l \le B} \text{Cov}\left(M_{\boldsymbol{\tau}_k}, M_{\boldsymbol{\tau}_l}\right)\end{aligned} \tag{9}$$

where

$$\begin{aligned}\text{Var}\left(M_{\boldsymbol{\tau}_b}\right) = &\sum_{i=1}^{N_{\text{cols}}} {a_{\boldsymbol{\tau}_b}}^2(\gamma_i)(1 - w_{i,j})^2 \text{Var}\left(g_\lambda(\gamma_i, v_j)\right) \\ &+ \sum_{i=1}^{N_{\text{cols}}} {a_{\boldsymbol{\tau}_b}}^2(\gamma_i) w_{i,j}^2 \text{Var}\left(g_\lambda(\gamma_i, v_{j+1})\right)\end{aligned} \tag{10}$$

and

$$\begin{aligned}\text{Cov}\left(M_{\boldsymbol{\tau}_k}, M_{\boldsymbol{\tau}_l}\right) = &\sum_{i=1}^{N_{\text{cols}}} a_{\boldsymbol{\tau}_k}(\gamma_i) a_{\boldsymbol{\tau}_l}(\gamma_i) V_{i,j}^{k,l} \text{Var}\left(g_\lambda(\gamma_i, v_{j_k})\right) \\ &+ \sum_{i=1}^{N_{\text{cols}}} a_{\boldsymbol{\tau}_k}(\gamma_i) a_{\boldsymbol{\tau}_l}(\gamma_i) W_{i,j}^{k,l} \text{Var}\left(g_\lambda(\gamma_i, v_{j_k+1})\right)\end{aligned} \tag{11}$$

with

$$V_{i,j}^{k,l} = (1 - w_{i,j_k})\left[(1 - w_{i,j_l})\delta_{j_k,j_l} + w_{i,j_l}\delta_{j_k,j_l+1}\right], \tag{12}$$

$$W_{i,j}^{k,l} = w_{i,j_k}\left[(1 - w_{i,j_l})\delta_{j_k+1,j_l} + w_{i,j_l}\delta_{j_k+1,j_l+1}\right], \tag{13}$$

and the Kronecker delta $\delta_{i,j}$ is 1 if $i = j$ and 0 otherwise. Equation 11 is obtained using the bilinearity of the covariance.

D. Experimental validation

Using the reconstruction toolkit (RTK), we simulated an acquisition centered around the diaphragm of the Forbild thorax phantom [5] with the geometry of the Siemens *Somatom go.Sim* CT scanner, a pitch of 0.8, 4 rotations and 360 projections per rotation. The variance was verified with a batch approach, using 10000 realizations of Poisson noise simulated before taking the logarithm with $I_0 = 5 \times 10^4$ photons/pixel in air. For each realization, the mean moments $\overline{M_{\lambda,\lambda'}}$ and $\overline{M_{\lambda',\lambda}}$ are computed for all pairs (λ, λ') where λ is a fixed reference projection. Their variance is calculated over all the realizations. The bandwidth parameter of the kernel was $\nu = 0.2$.

III. Results

The top plot of Figure 2 shows the variance of $\overline{M_{\lambda,\lambda'}}$ and $\overline{M_{\lambda',\lambda}}$ for all pairs obtained with the theoretical formula (Equation 9) and the batch approach with 10000 realizations. The two sets of curves match with a mean relative error of 0.012 for $\text{Var}(\overline{M_{\lambda,\lambda'}})$ and 0.011 for $\text{Var}(\overline{M_{\lambda',\lambda}})$. The two projections of a pair with an absolute source angle difference close to $0°$ and $180°$ are roughly similar and noise impacts their moments similarly. When the absolute difference is about $90°$ or $270°$, the elliptic shape of the Forbild thorax phantom implies significantly different projections, noise and moments variance.

The consistency metric for the noiseless acquisition and the mean of the consistency metric taken over 10 000 realizations of noisy data, referred to as the mean absolute error (MAE), is shown at the bottom plot of Figure 2. DCC are very sensitive to noise when the baseline intersects the object (gray areas). The largest inconsistencies visible in both noiseless and noisy moment curves are attributed to systematic sampling and interpolation errors. The MAE follows quite well the standard deviation (STD) of the mean moments difference for pairs with absolute gantry difference around $0°$ and $180°$ but not for pairs with absolute gantry difference around $90°$ or $270°$ (see vertical black lines in Figure 2 bottom plot). This difference is caused by a noise-induced bias due to the non-linearity of the logarithm which increases the error measured by the inconsistency metric. This bias is larger for lateral projections than antero-posterior ones because in these projections, the

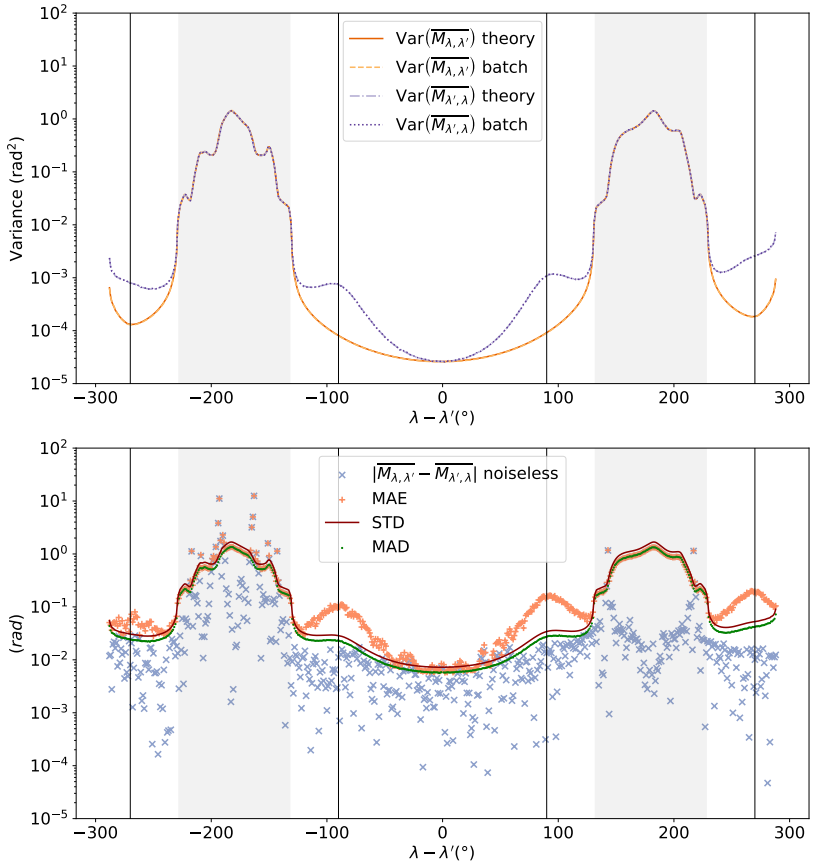

Fig. 2: Top plot: variance validation results. Bottom plot: illustration of the cone-beam pair-wise DCC.

photons are more attenuated. The logarithm decreases greatly for a small number of photons leading to a higher bias than for a high number of photons.

The MAE would be the mean absolute deviation of the moments difference if the mean were zero. For a normal distribution, the ratio of the mean absolute deviation to the standard deviation is equal to $\sqrt{2/\pi}$. The ratio of the MAE over STD deviates from this value due to the noise-induced bias. In the bottom plot of Figure 2, we also computed the mean absolute deviation (MAD) of the moments difference with respect to the mean of the consistency metric over the 10^4 realizations. The ratio MAD/STD is approximately constant for all pairs (λ, λ') and equals $\sqrt{2/\pi}$ which shows that the noise not only impacts the variance of the consistency metric but also its average.

IV. Discussion and Conclusions

We proposed a theoretical formula of the variance for cone-beam pair-wise DCC in helical CT and validated it with batch simulations. The resulting formula explains the observed variability of the DCC depending on the angular distance between source positions. The other differences were explained by discretization errors or the noise-induced bias for projections with a low number of photons. For example, the variance is several orders of magnitude larger when the baseline (defined by the two source positions) intersects the object. Prediction of the DCC variance should therefore be accounted for in DCC-based estimation algorithms.

References

[1] J. Wang, T. Li, H. Lu and Z. Liang, "Penalized weighted least-squares approach to sinogram noise reduction and image reconstruction for low-dose X-ray computed tomography," IEEE Transactions on Medical Imaging, vol. 25, no. 10, pp. 1272–1283, 2006.

[2] A. Wunderlich and F. Noo, "Image covariance and lesion detectability in direct fan-beam x-Ray computed tomography," Physics in medicine and biology, vol. 53, pp. 2471–2493, 2008.

[3] M. Mouchet, "Breathing motion detection in computed tomography using data consistency conditions," Ph.D dissertation, INSA de Lyon, Université de Lyon, Lyon, 2022.

[4] R. Clackdoyle, "Necessary and sufficient consistency conditions for fan-beam projections along a line," IEEE Transactions on Nuclear Science, vol. 60, pp. 1560–1569, 2013.

[5] F. Bergner and M. Kachelrieß, "4D generalized thorax phantom," Institute of Medical Physics (IMP), Friedrich-Alexander-University of Erlangen-Nürnberg, Tech. Rep., 2009.